Two-Dimensional Linear Implicit Relaxed Scheme for Hyperbolic Conservation Laws

Angelo Iollo, Gabriella Puppo, Andrea Thomann

Two-Dimensional Linear Implicit Relaxed Scheme for Hyperbolic Conservation Laws

Angelo Iollo, Gabriella Puppo, and Andrea Thomann

Abstract We present a two-dimensional extension to the linear implicit all-speed finite volume scheme for hyperbolic conservation laws based on Jin-Xin relaxation recently forwarded in [6]. It is based on stiffly accurate SDIRK methods in time and a convex combination of Rusanov and centered fluxes in space making it asymptotically consistent in the low Mach number regime and allows an accurate capturing of material waves under large time steps. The scheme is numerically tested on the Euler equations and a non-linear model for elasticity in the compressible and low Mach number regime.

Keywords All-speed scheme · Relaxation method · Eulerian elasticity · Linearly implicit schemes

1 Introduction

The importance of implicit schemes in the numerical integration of evolutionary equations typically lies in the possibility of circumventing the limitations imposed by the amplification of numerical instabilities from which explicit schemes suffer.

G. P. acknowledges the support of PRIN2017 and Sapienza, Progetto di Ateneo RM120172 B41DBF3A.

A. Iollo (✉)
IMB, Université Bordeaux and Equipe-projet Memphis, Inria Bordeaux-Sud Ouest, Bordeaux, France
e-mail: angelo.iollo@inria.fr

G. Puppo
Institute of Mathematics, La Sapienza Università di Roma, Roma, Italy
e-mail: gabriella.puppo@uniroma1.it

A. Thomann
Université de Strasbourg, CNRS, Inria, IRMA, F-67000 Strasbourg, France
e-mail: andrea.thomann@inria.fr

E. Franck et al. (eds.), *Finite Volumes for Complex Applications X—Volume 2, Hyperbolic and Related Problems*, Springer Proceedings in Mathematics & Statistics 433,
https://doi.org/10.1007/978-3-031-40860-1_18

Added to this motivation is, in the case of hyperbolic models, the need to preserve the consistency and accuracy of the integration scheme when the propagation phenomena described by the model have largely incomparable velocity scales. Nevertheless, an implicit scheme involves the inversion of a large often non linear system and, what is worse, the calculation of the Jacobian of the scheme residuals. The latter operation can be (i) cumbersome—when the numerical flux is non linear and the constitutive law complex; (ii) ill-posed—in presence of discontinuous solutions; (iii) limiting—if one wishes to devise a scheme independent of the constitutive laws of the model.

This work is in the wake of previous contributions in which the hyperbolic model considered is equivalent [2, 8], in the limit of an ad hoc relaxation, to a model in which the differential operator is linear and where the nonlinearity is transferred into the source term. This allows to resort to an implicit integration approach in which part of the difficulties enunciated above (the linear system is still there) can be overcome. Unlike other approaches, however, what is proposed below does not depend on relaxation parameters since it is an implicit relaxed scheme. Moreover, unlike previously, see [1, 7], the proposed implicit relaxed scheme does not involve additional relaxation variables due to a prediction-correction type technique projecting the relaxation source terms on the zero relaxation limit.

In what follows, the main contribution with respect to the work of [6] is the extension of the scheme to two-dimensional problems for compressible hyperelastic material flows in all-Mach regimes.

2 The Jin-Xin Relaxation Method

We consider the following hyperbolic conservation law on the two-dimensional domain Ω given by

$$\partial_t \boldsymbol{\psi} + \partial_x \boldsymbol{f}^x(\boldsymbol{\psi}) + \partial_y \boldsymbol{f}^y(\boldsymbol{\psi}) = 0, \tag{1}$$

with the state vector $\boldsymbol{\psi} \in \mathbb{R}^k$, directional fluxes $\boldsymbol{f}^x$, $\boldsymbol{f}^y : \mathbb{R}^k \to \mathbb{R}^k$. Following [5], we introduce a vector of relaxation variables $\boldsymbol{v} \in \mathbb{R}^k$ and consider the following relaxation system given by

$$\partial_t \boldsymbol{\psi} + \partial_x \boldsymbol{v} + \partial_y \boldsymbol{w} = 0, \tag{2a}$$

$$\partial_t \boldsymbol{v} + \boldsymbol{A}_x^2 \partial_x \boldsymbol{\psi} = -\frac{1}{\eta}\left(\boldsymbol{v} - \boldsymbol{f}^x(\boldsymbol{\psi})\right), \tag{2b}$$

$$\partial_t \boldsymbol{w} + \boldsymbol{A}_y^2 \partial_x \boldsymbol{\psi} = -\frac{1}{\eta}\left(\boldsymbol{w} - \boldsymbol{f}^y(\boldsymbol{\psi})\right), \tag{2c}$$

where $\eta > 0$ denotes the relaxation rate and $\boldsymbol{A}_x^2$, $\boldsymbol{A}_y^2$ are diagonal matrices with positive entries given by

$$\boldsymbol{A}_x^2 = \mathrm{diag}(a_x^2, \cdots, a_x^2), \quad \boldsymbol{A}_y^2 = \mathrm{diag}(a_y^2, \cdots, a_y^2). \tag{3}$$

The fluxes on the relaxation model are linear whereas the relaxation source terms on the right hand side of (2a) are non-linear and stiff for small η. Rewriting Eqs. (2b), (2c), using a Chapman-Enskog expansion of the relaxation variables for small η, we find

$$\boldsymbol{v} = \boldsymbol{f}^x(\boldsymbol{\psi}) - \eta(\nabla_{\boldsymbol{\psi}} \boldsymbol{f}^x(\boldsymbol{\psi})^2 - \boldsymbol{A}_x^2))\partial_x \boldsymbol{\psi}, \tag{4a}$$

$$\boldsymbol{w} = \boldsymbol{f}^y(\boldsymbol{\psi}) - \eta(\nabla_{\boldsymbol{\psi}} \boldsymbol{f}^y(\boldsymbol{\psi})^2 - \boldsymbol{A}_y^2))\partial_y \boldsymbol{\psi}, \tag{4b}$$

where $\nabla_{\boldsymbol{\psi}} \boldsymbol{f}^x(\boldsymbol{\psi}), \nabla_{\boldsymbol{\psi}} \boldsymbol{f}^x(\boldsymbol{\psi})$ denote the Jacobians of the flux functions $\boldsymbol{f}^x, \boldsymbol{f}^y$ respectively. We have neglected the $\mathcal{O}(\eta^2)$ terms in the expansion (4a), since we are only interested in the first order diffusion terms in η. Inserting (4a) into (2a), we have

$$\partial_t \boldsymbol{\psi} + \partial_x \boldsymbol{f}(\boldsymbol{\psi}) = \eta \left(\partial_x \left(\left(\boldsymbol{A}_x^2 - \nabla_{\boldsymbol{\psi}} \boldsymbol{f}^x(\boldsymbol{\psi}) \right) \partial_x \boldsymbol{\psi} \right) + \partial_y \left(\left(\boldsymbol{A}_y^2 - \nabla_{\boldsymbol{\psi}} \boldsymbol{f}^y(\boldsymbol{\psi})^2 \right) \partial_y \boldsymbol{\psi} \right) \right).$$

To obtain a diffusive approximation of the original system of Eq. (1), it has to be ensured that the diffusion term on the right hand side is non-negative. This yields the so called sub-characteristic condition, that for all $\boldsymbol{\psi}$ it has to hold $\boldsymbol{A}_x^2 - \nabla_{\boldsymbol{\psi}} \boldsymbol{f}^x(\boldsymbol{\psi}) \geq 0$ and $\boldsymbol{A}_y^2 - \nabla_{\boldsymbol{\psi}} \boldsymbol{f}^y(\boldsymbol{\psi})^2 \geq 0$. This positive semi-definite restriction is fulfilled for the choice (3) with

$$a_x = \max_{\boldsymbol{x} \in \Omega} \max_{j=1,\ldots,k} |\lambda_j^x(\boldsymbol{\psi}(\boldsymbol{x}, t))|, \quad a_y = \max_{\boldsymbol{x} \in \Omega} \max_{j=1,\ldots,k} |\lambda_j^y(\boldsymbol{\psi}(\boldsymbol{x}, t))|, \tag{5}$$

where $\lambda_j^x, \lambda_j^y, \ j = 1, \ldots, k$ are the characteristic speeds of the original Eq. (1) given by the eigenvalues of the directional Jacobians $\nabla_{\boldsymbol{\psi}} \boldsymbol{f}^x(\boldsymbol{\psi}), \nabla_{\boldsymbol{\psi}} \boldsymbol{f}^y(\boldsymbol{\psi})$. Thus from (4a) we recover at leading order the original system, namely

$$\boldsymbol{v} = \boldsymbol{f}^x(\boldsymbol{\psi}), \ \boldsymbol{w} = \boldsymbol{f}^y(\psi), \quad \partial_t \boldsymbol{\psi} + \partial_x \boldsymbol{f}^x(\boldsymbol{\psi}) + \partial_y \boldsymbol{f}^y(\boldsymbol{\psi}) = 0, \tag{6}$$

also referred to as the relaxation limit.

3 The Numerical Scheme

Following the lines of construction of the one-dimensional scheme introduced in [6], we use stiffly accurate singular diagonally implicit Runge-Kutta (SA-SDIRK) methods in a finite volume framework. To exploit the linear fluxes of the relaxation system (2), we apply an operator splitting to separate the non-linear relaxation source terms from the linear right hand side. For each stage $k = 1, \ldots, s$ of an s-stages Runge-Kutta method we have

$$\begin{cases} \boldsymbol{\psi}^\star &= \boldsymbol{\psi}^n \\ \boldsymbol{v}^\star &= \boldsymbol{v}^n - \frac{\Delta t}{\eta}\left(\boldsymbol{v}^\star - \boldsymbol{f}^x(\boldsymbol{\psi}^\star)\right), \\ \boldsymbol{w}^\star &= \boldsymbol{w}^n - \frac{\Delta t}{\eta}\left(\boldsymbol{w}^\star - \boldsymbol{f}^y(\boldsymbol{\psi}^\star)\right), \end{cases} \tag{7}$$

where $\boldsymbol{\psi}^\star$, $\boldsymbol{v}^\star$, $\boldsymbol{w}^\star$ denote the states after the relaxation process. Taking the limit $\eta \to 0$, we obtain $\boldsymbol{v}^\star = \boldsymbol{f}^x(\boldsymbol{\psi}^\star)$, $\boldsymbol{w}^\star = \boldsymbol{f}^y(\boldsymbol{\psi}^\star)$ which is consistent with the relaxation equilibrium solution (6). On the homogeneous left hand side of (2) we apply a SDIRK method with weights α_{jl}, β_j, $j = 1, \ldots, s$, $l = 1, \ldots j-1$, yielding

$$\begin{cases} \boldsymbol{\psi}^{(j)} &= \boldsymbol{\psi}^n - \Delta t \sum_{l=1}^{j} \alpha_{jl}\left(\partial_x \boldsymbol{v}^{(l)} + \partial_y \boldsymbol{w}^{(l)}\right), \\ \boldsymbol{v}^{(j)} &= \boldsymbol{v}^n - \Delta t \sum_{l=1}^{j} \alpha_{jl} \boldsymbol{A}_x^2 \partial_x \boldsymbol{\psi}^{(l)}, \\ \boldsymbol{w}^{(j)} &= \boldsymbol{w}^n - \Delta t \sum_{l=1}^{j} \alpha_{jl} \boldsymbol{A}_y^2 \partial_y \boldsymbol{\psi}^{(l)}, \end{cases} \tag{8a}$$

$$\begin{cases} \boldsymbol{\psi}^{n+1} &= \boldsymbol{\psi}^n - \Delta t \sum_{j=1}^{s} \beta_j\left(\partial_x \boldsymbol{v}^{(j)} + \partial_y \boldsymbol{w}^{(j)}\right), \\ \boldsymbol{v}^{n+1} &= \boldsymbol{v}^n - \Delta t \sum_{j=1}^{s} \beta_j \boldsymbol{A}_x^2 \partial_x \boldsymbol{\psi}^{(j)}, \\ \boldsymbol{w}^{n+1} &= \boldsymbol{w}^n - \Delta t \sum_{j=1}^{s} \beta_j \boldsymbol{A}_y^2 \partial_y \boldsymbol{\psi}^{(j)}. \end{cases} \tag{8b}$$

Note that this system has thrice as many variables per stage and update as the original system (1). To reduce the computational overhead associated with these additional auxiliary variables, we replace the stages $\boldsymbol{v}^{(l)}$, $\boldsymbol{w}^{(l)}$ in the update for $\boldsymbol{\psi}^{(j)}$ in (8a) and obtain the time-semi discrete stages

$$\begin{aligned} \boldsymbol{\psi}^{(j)} \; & -\Delta t^2 \alpha_{jj}^2 \left(\boldsymbol{A}_x^2 \partial_x^2 \boldsymbol{\psi}^{(j)} + \boldsymbol{A}_y^2 \partial_y^2 \boldsymbol{\psi}^{(j)}\right) = \\ \boldsymbol{\psi}^n \; & -\Delta t \alpha_{jj} \partial_x \boldsymbol{v}^n - \Delta t \sum_{l=1}^{j-1} \alpha_{jl} \partial_x \boldsymbol{v}^{(l)} + \Delta t^2 \alpha_{jj} \sum_{l=1}^{j-1} \alpha_{jl} \boldsymbol{A}_x^2 \partial_x^2 \boldsymbol{\psi}^{(l)} \\ & -\Delta t \alpha_{jj} \partial_y \boldsymbol{w}^n - \Delta t \sum_{l=1}^{j-1} \alpha_{jl} \partial_y \boldsymbol{w}^{(l)} + \Delta t^2 \alpha_{jj} \sum_{l=1}^{j-1} \alpha_{jl} \boldsymbol{A}_y^2 \partial_y^2 \boldsymbol{\psi}^{(l)}. \end{aligned} \tag{9}$$

Using the fact, that from the relaxation source terms we have $\boldsymbol{v}^n = \boldsymbol{f}^x(\boldsymbol{\psi}^n)$, $\boldsymbol{v}^{(l)} = \boldsymbol{f}^x(\boldsymbol{\psi}^{(l)})$, $\boldsymbol{w}^n = \boldsymbol{f}^y(\boldsymbol{\psi}^n)$, $\boldsymbol{w}^{(l)} = \boldsymbol{f}^y(\boldsymbol{\psi}^{(l)})$ for all previous stages $l = 1, \ldots, j-1$, it follows

$$\begin{aligned} \boldsymbol{\psi}^{(j)} \; & -\Delta t^2 \alpha_{jj}^2 \left(\boldsymbol{A}_x^2 \partial_x^2 \boldsymbol{\psi}^{(j)} + \boldsymbol{A}_y^2 \partial_y^2 \boldsymbol{\psi}^{(j)}\right) = \\ \boldsymbol{\psi}^n \; & -\Delta t \alpha_{jj} \partial_x \boldsymbol{f}^x(\boldsymbol{\psi}^n) - \Delta t \sum_{l=1}^{j-1} \alpha_{jl} \partial_x \boldsymbol{f}^x(\boldsymbol{\psi}^{(l)}) + \Delta t^2 \alpha_{jj} \sum_{l=1}^{j-1} \alpha_{jl} \boldsymbol{A}_x^2 \partial_x^2 \boldsymbol{\psi}^{(l)} \\ & -\Delta t \alpha_{jj} \partial_y \boldsymbol{f}^y(\boldsymbol{\psi}^n) - \Delta t \sum_{l=1}^{j-1} \alpha_{jl} \partial_y \boldsymbol{f}^y(\boldsymbol{\psi}^{(l)}) + \Delta t^2 \alpha_{jj} \sum_{l=1}^{j-1} \alpha_{jl} \boldsymbol{A}_y^2 \partial_y^2 \boldsymbol{\psi}^{(l)}, \end{aligned}$$

thus only depending on the state variable $\boldsymbol{\psi}$ and from the relaxation source term we obtain $\boldsymbol{v}^{(j)} = \boldsymbol{f}^x(\boldsymbol{\psi}^{(j)})$, $\boldsymbol{w}^{(j)} = \boldsymbol{f}^y(\boldsymbol{\psi}^{(j)})$. Note, that the implicit system (10) decouples into k implicit subsystems for each state variable in $\boldsymbol{\psi}$, since $\boldsymbol{A}_x$ and $\boldsymbol{A}_y$ are diagonal matrices. Moreover, the coefficient matrices for each implicit subsystems are identical M-matrices since we use SDIRK methods. This drastically reduces the computational overhead compared to coupled implicit systems based on linearizations of Jacobians, see e.g. [1, 7]. Finally we obtain for the update

$$\boldsymbol{\psi}^{n+1} = \boldsymbol{\psi}^n - \Delta t \sum_{j=1}^{s} \beta_j \left(\partial_x \boldsymbol{f}^x(\boldsymbol{\psi}^{(j)}) + \partial_y \boldsymbol{f}^y(\boldsymbol{\psi}^{(j)}) \right). \tag{10}$$

In space we consider the two-dimensional domain $\Omega \subset \mathbb{R}^2$ paved with rectangular cells $\Omega_I = [x_{i-/2}, x_{i+1/2}] \times [y_{j-1/2}, y_{j-1/2}]$ of length Δx, Δy in x-and y-direction respectively with barycenter $(x_i, y_j) = (i\Delta x, j\Delta y)$. According to the finite volume framework, we evolve cell averages defined by

$$\boldsymbol{\psi}_I^n = \frac{1}{|\Omega_I|} \int_{\Omega_I} \boldsymbol{\psi}(x, y, t^n) d\Omega. \tag{11}$$

The finite volume scheme is then given by

$$\begin{aligned}
\boldsymbol{\psi}_I^{(j)} \; & -\Delta t^2 \alpha_{jj}^2 \left(\boldsymbol{A}_x^2 \mathcal{D}_x^{(j)} + \boldsymbol{A}_y^2 \mathcal{D}_y^{(j)} \right) = \qquad (12) \\
\boldsymbol{\psi}_I^n \; & -\Delta t \alpha_{jj} \mathcal{F}_x^n - \Delta t \sum_{l=1}^{j-1} \alpha_{jl} \mathcal{F}_x^{(l)} + \Delta t^2 \alpha_{jj} \sum_{l=1}^{j-1} \alpha_{jl} \boldsymbol{A}_x^2 \mathcal{D}_x^{(l)} \\
& -\Delta t \alpha_{jj} \mathcal{F}_y^n - \Delta t \sum_{l=1}^{j-1} \alpha_{jl} \mathcal{F}_y^{(l)} + \Delta t^2 \alpha_{jj} \sum_{l=1}^{j-1} \alpha_{jl} \boldsymbol{A}_y^2 \mathcal{D}_y^{(l)}, \\
\boldsymbol{\psi}^{n+1} \; & = \boldsymbol{\psi}^n - \Delta t \sum_{j=1}^{s} \beta_j \left(\mathcal{F}_x^{(j)} + \mathcal{F}_y^{(j)} \right) \qquad (13)
\end{aligned}$$

with the discretized diffusion operators $\mathcal{D}$ and numerical fluxes $\mathcal{F}$, given by

$$\mathcal{D}_x = \frac{1}{\Delta x^2} \left(\boldsymbol{\psi}_{i+1,j} - 2\boldsymbol{\psi}_{i,j} + \boldsymbol{\psi}_{i-1,j} \right), \quad \mathcal{D}_y = \frac{1}{\Delta y^2} \left(\boldsymbol{\psi}_{i,j+1} - 2\boldsymbol{\psi}_{i,j} + \boldsymbol{\psi}_{i,j-1} \right),$$
$$\mathcal{F}_x = \frac{1}{\Delta x} \left(\boldsymbol{f}^x_{i+1/2,j} - \boldsymbol{f}^x_{i-1/2,j} \right), \quad \mathcal{F}_y = \frac{1}{\Delta y} \left(\boldsymbol{f}^y_{i,j+1/2} - \boldsymbol{f}^y_{i,j-1/2} \right).$$

The fluxes at the interface are approximated by a convex combination between centered and Rusanov fluxes based on the local Mach number M_{loc} given by the ratio between local fluid and sound speed. They read e.g.

$$\boldsymbol{f}^x_{i+1/2,j} = \frac{1}{2}\left(\boldsymbol{f}^x(\boldsymbol{\psi}_{i+1,j}) + \boldsymbol{f}^x(\boldsymbol{\psi}_{i,j})\right) - a_{i+1/2,j}\theta\left(M_{\text{loc}}\right)(\boldsymbol{\psi}_{i+1,j} - \boldsymbol{\psi}_{i,j}), \tag{14}$$

with the local maximal characteristic speed

$$a_{i+1/2,j} = \max_l(|\lambda_l(\boldsymbol{\psi}(x_i, y_j, t^n))|, |\lambda_l(\boldsymbol{\psi}(x_{i+1}, y_j, t^n))|)$$

and an indicator function, e.g.,

$$\theta\left(M_{\text{loc}}\right) = \sin\left(\frac{\pi M_{loc}}{2}\right) \text{ for } M_{loc} \in [0,1] \quad \text{and} \quad \theta\left(M_{\text{loc}}\right) = 1 \text{ for } M_{loc} > 1.$$

This choice ensures the correct numerical diffusion for almost incompressible flows (centered) in the low Mach number limit and compressible flows (upwind scheme based on Rusanov fluxes with $M_{\text{loc}} \approx 1$). This, together with SA-SDIRK time integration, ensures an accurate description of low Mach flows, as well as compressible flows thus (12), (13) constitutes an *all-speed scheme*. In consequence, by construction, the numerical scheme is *asymptotic preserving* due to asymptotic stable time integrators and centered numerical fluxes in the low Mach number limit.

4 Numerical Results and Discussion

In the following, we use a first order scheme consisting the backward Euler scheme in time and a two stage second order SA-SDIRK method with $\alpha_{jj} = 1 - \sqrt{2}/2$ with a minmod reconstruction at the cell interfaces to ensure second order in space also for compressible flows. We test the numerical schemes on the Euler equations with an ideal gas law and a conservative model of non-linear elasticity given by

$$\boldsymbol{\psi} = \begin{pmatrix} \rho \\ \rho\boldsymbol{u} \\ [\nabla Y] \\ E \end{pmatrix}, \quad \boldsymbol{f}(\boldsymbol{\psi}) = \begin{pmatrix} \rho\boldsymbol{u} \\ \rho\boldsymbol{u}\otimes\boldsymbol{u} - \sigma \\ \boldsymbol{u}\cdot[\nabla Y]\mathbb{I} \\ \boldsymbol{u}(E+p) \end{pmatrix} \tag{15}$$

from which the directional fluxes $\boldsymbol{f}^x, \boldsymbol{f}^y$ in (2) can be deduced. It consists of conservation of mass ρ, momentum $\rho\boldsymbol{u}$ and total energy $E = \rho e + 1/2\rho|\boldsymbol{u}|^2$ with an additional evolution equation for the deformation gradient $[\nabla Y]$. We consider a neo-hookean equation of state $\rho e = (\gamma - 1)p + p_\infty + \chi(\text{tr}\bar{B} - 2)$ where p_∞, χ are material constants and $\bar{B}$ is the normalized Cauchy stress tensor $\bar{B} = \det([\nabla Y])([\nabla Y]^{-1}[\nabla Y]^{-T})$ and the stress tensor σ is given by

$$\sigma = -p + 2\chi\det([\nabla Y])\left(\bar{B} - \frac{\text{tr}\bar{B}}{2}\mathbb{I}\right). \tag{16}$$

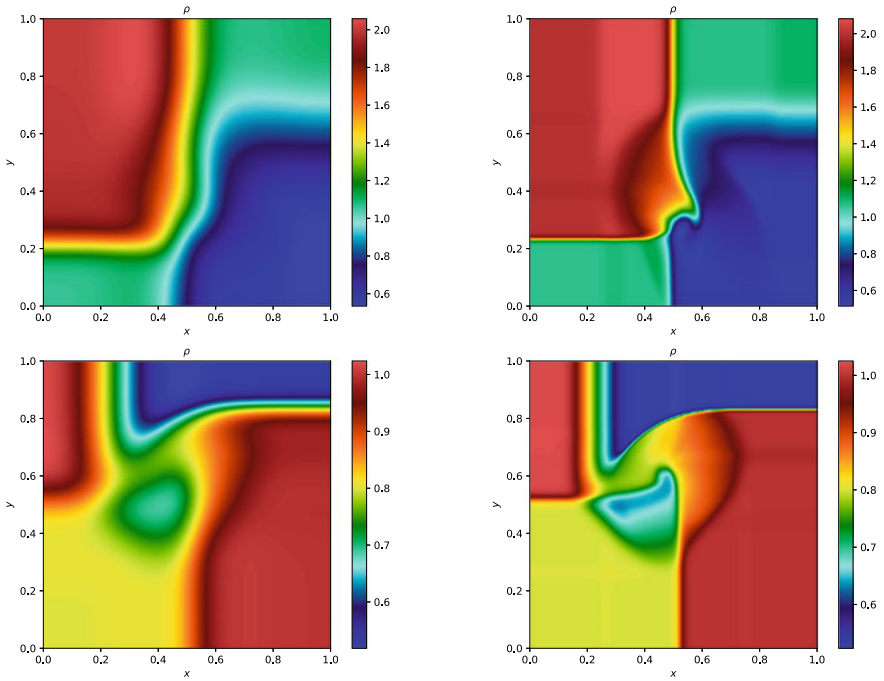

Fig. 1 Riemann Problems for Euler equations in the compressible regime from [4] on a grid of 256×256 cells: Top panel: density for RP CRCS at time $T_f = 0.3$. Bottom panel: density for RP RCCS at time $T_f = 0.2$. Left side: first order scheme. Right side: Second order scheme

For more details on the model and its derivation see [2, 8]. Note that for $p_\infty = 0$ and $\chi = 0$. we recover the standard Euler equations with an ideal gas law.

Compressible Riemann Problems We consider two 2D Riemann Problems (RPs) for the Euler equations with an ideal gas law and $\gamma = 1.4$ taken from [4] containing contact discontinuities. Since both cases are in the compressible regime, we apply an acoustic CFL condition with CFL number 0.9 to *follow all waves* in the model. The first test consists of a contact, shock, contact and rafaction wave (RP CSCR) in counterclockwise rotation starting from the top right quarter. The second one consists of a rarefaction, two contacts and a shock wave (RP RCCS), both displayed in Fig. 1. Since the scheme contains the full upwind diffusion, the first order scheme is quite diffusive on all waves, whereas the second order scheme captures all waves accurately.

Gresho Vortex Next, we consider the Gresho vortex, which is a solution to the incompressible Euler equations with a divergence free velocity field and constant initial density and is a stationary exact solution to the Euler equations. For the set-up see e.g. [3]. We run it for three different Mach regimes on a gird of 40×40 on the domain $[0, 1]^2$ with $\Delta t = 2.2 \cdot 10^{-2}$. It is especially suited to verify the AP property,

Table 1 Gresho vortex: L^1 error of the density at final time $T = 1$ with respect to initial constant density $\rho(x, 0) = 1$ and ratio of kinetic energy over the computational domain $[0, 1]^2$ for different Mach number regimes

	Scheme	$M_{\max} = 10^{-2}$	$M_{\max} = 10^{-4}$	$M_{\max} = 10^{-6}$
L^1 error ρ	First order	9.91e-8	8.77e-12	1.43e-15
	Second order	6.88e-7	2.11e-11	3.64e-15
$E^T_{\text{kin}}/E^0_{\text{kin}}$	First order	0.998128	0.999945	0.999946
	Second order	0.999941	0.999945	0.999952

since the kinetic energy is preserved. Thus the loss of kinetic energy indicates the diffusiveness of the numerical scheme reported in Table 1. As we see, for all Mach regimes, the loss due to diffusion is almost equal and the numerical solutions resemble quite accurately the initial exact solution of the vortex. Moreover we present the L^1 error of the density at the final time with respect to the initial density which is, due to the stationary aspect of the test case, even of order M^3 thus the solution formally converges to the incompressible limit solution as the Mach number decreases which numerically verifies the AP property of the scheme.

Deformation of hyperelastic solids Finally, we consider two RPs concerning the deformation of compressible solids (15) taken from [1] which exhibits two longitudinal, two shear waves and a material wave. We consider two materials, copper with $p_\infty = 3.42 \cdot 10^{10}$, $\gamma = 4.33$ and shear modulus $\chi = 5 \cdot 10^{10}$ which lies in the low acoustic and low shear Mach number regime, i.e. the longitudinal and shear waves are considerably faster than the material wave. The initial condition consists of a jump in pressure from 10^9 to 10^5 in the bottom right quarter of the domain under constant density of 8900 and a zero velocity field. The second material under consideration is rubber ($p_\infty = 6.8 \cdot 10^8$, $\gamma = 4.4$, $\chi = 8 \cdot 10^5$) which lies in the low acoustic Mach number regime where the longitudinal waves are significantly faster than the shear and material waves. The initial condition consists of a jump in pressure from 10^8 to $9.8 \cdot 10^7$ and velocities from 0 to 20 in the bottom right quarter of the domain under constant density of 1000. The numerical results for our implicit first and second order scheme, as well as an explicit SSP-RK2 scheme, with 256^2 grid cells on a $[0, 2]^2$ domain are presented in Fig. 2 with $\Delta t = 1.17 \cdot 10^{-5}$ for copper and $\Delta t = 2.08 \cdot 10^{-5}$ for rubber. Note, that the second order explicit upwind scheme requires a time step of $\Delta t = 3.3 \cdot 10^{-7}$ for copper and $1.8 \cdot 10^{-6}$ for rubber. Our implicit first and second order schemes capture the resulting contact wave in the density accurately, in contrast to the explicit method, while diffusing shear and longitudinal waves. Due to the higher order approximation, we observe small oscillations on the negligible fast waves in our second order scheme.

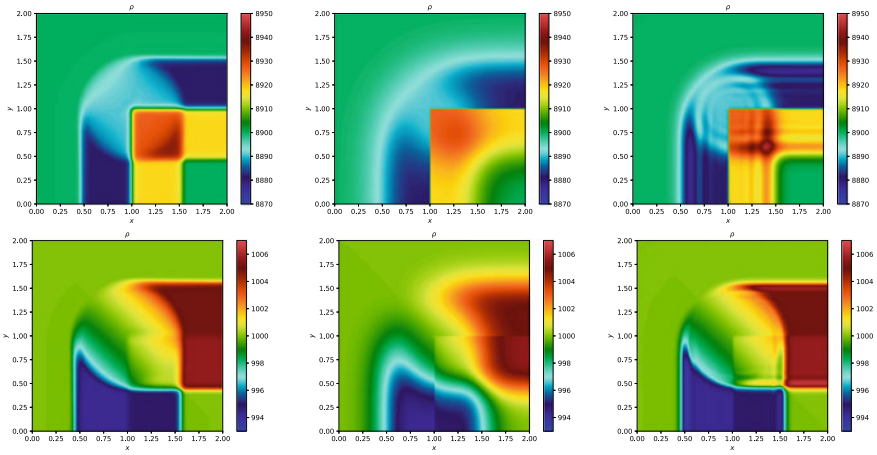

Fig. 2 Riemann Problem elastic solids on the domain $[0, 2]^2$: Top panel: Copper density at time $T = 10^{-4}$. Bottom panel: Rubber density at time $T = 3 \cdot 10^{-4}$. Left: Explicit second order scheme. Middle: Our first order scheme. Right: Our second order scheme

References

1. Abbate, E., Iollo, A., Puppo, G.: An asymptotic-preserving all-speed scheme for fluid dynamics and nonlinear elasticity. SIAM J. Sci. Comput. **41**, A2850–A2879 (2019)
2. de Brauer, A., Iollo, A., Milcent, T.: A Cartesian scheme for compressible multimaterial models in 3d. J. Comput. Phys. **313**, 121–143 (2016)
3. Miczek, F., Friedrich, K.R., Edelmann, P.V.F.: New numerical solver for flows at various Mach numbers. Astron. & Astrophys. **576**, A50 (2015)
4. Kurganov, A., Tadmor, E.: Solution of two-dimensional Riemann problems for gas dynamics without Riemann problem solvers. Numer. Methods Part. Differ. Equ. Int. J. **18**(5), 584–608 (2002)
5. Jin, S., Xin, Z.: The relaxation schemes for systems of conservation laws in arbitrary space dimensions. Commun. Pur. Appl. Math. **48**, 235–276 (1995)
6. Thomann, A., Iollo, A., Puppo, G.: Implicit relaxed all Mach number schemes for gases and compressible materials. SIAM J. Sci. Comput. (2021). arXiv.org/abs/2112.14126
7. Abbate, E., Iollo, A., Puppo, G.: An all-speed relaxation scheme for gases and compressible materials. J. Comput. Phys. **351**, 1–24 (2017)
8. Gorsse, Y., Iollo, A., Milcent, T., Telib, H.: A simple Cartesian scheme for compressible multimaterials. J. Comput. Phys. **272**, 772–798 (2014)